A New Numerical Analysis of Line Equations Considering Corona Loss on Single-Conductor System

By

Jūrō UMOTO* and Takehisa HARA**

(Received December 6, 1967)

It is very important to investigate the wave attenuation and distortion due to corona discharge, for the purpose of solving successfully the surge problems on the ultra-high voltage transmission systems. So, in this paper, from the nonlinear line equations considering corona loss on a single-conductor system, the author derived a new ditigal calculation to analyse the attenuation and distortion of the travelling waves caused by corona discharge on a single-conductor system, which is founded on their surge analyser considering corona loss. Then, they compared their digital computation results with the experimental ones on the artificial transmission line by the other researchers and they could successfully elect the optimum values of the corona loss constants of the positive and negative travelling waves.

1. Introduction

The values of the lightning surge voltages on the transmission systems often are over the ones of the critical corona voltages of the line conductors, and in such cases the travelling waves are distorted and attenuated due to corona loss. Therefore it is very important to investigate not only the wave distortion and attenuation by the skin effects of the lines and the ground return, but also those caused by the corona discharge from the conductor surface, through the line equations.

In this view, already the authors have invented a surge analyser[1)~4)] considering the corona loss, and they introduced a digital computation method[5)] founded on this analyser. But it is difficult to produce the pure lumped inductance (L)-capacitance (C) delay line which is the fundamental circuit of the surge analyser, since the actual inductance coil has a resistance, and so the computation errors may be developed, as the surge considerably attenuate due to the proper L-C line loss. Moreover we have great trouble in exchanging the capacitors and resistors which make up the corona loss elements in the surge analyser, when the corona loss constants are changed.

* Department of Electrical Engineering.
** Department of Electrical Engineering, II.

Now, in this paper, we show the numerical calculation of attenuation and distortion of the surge on a single conductor due to the corona loss and elect the optimum values of the corona loss constants for the surge by comparing the computed results with the experimental ones obtained[6] by Fujitaka and others on a mimic experimental transmission line, and we compare and investigate them with the results by surge analyser which have been previously obtained by the authors.

2. Numerical Analysis of Line Equations Considering Corona Loss

2.1. Line Equations Considering Corona Loss

On the assumption that the formula of the square characteristics for the alternating current corona loss of the wire given by Peek is yet the reasonable one to the corona loss with respect to travelling waves, the line equations were modified by the authors, so that the wave attenuation and distortion by the corona loss may be analyzed more favourably than before, as follows.

$$\left.\begin{aligned} -\frac{\partial v}{\partial x} &= L\frac{\partial i}{\partial t}, \\ -\frac{\partial i}{\partial x} &= C\frac{\partial v}{\partial t}+Kv_{co}\eta+kv_{co}\frac{\partial \zeta}{\partial t}, \end{aligned}\right\} \qquad (1)$$

where

$$\left.\begin{aligned} &\eta = \begin{cases} 0, & 0\leq\xi<1, \\ (\xi-1)^2/\xi, & \xi\geq 1, \end{cases} \\ &\zeta = \begin{cases} 0, & 0\leq\xi<1, \\ 2(\xi-1-\log\xi), & \xi\geq 1, \end{cases} \\ &\xi = v/v_{co}, \\ &v_{co} \quad : \text{corona voltage}, \\ &v \text{ and } i \ : \text{voltage and current at distant } x \text{ from initial point}, \\ &L \text{ and } C\text{: inductance and capacitance of line per unit length}, \\ &K = k(f+25) = \sigma_G\sqrt{r/2h}\times 10^{-11} \ [\mho/\mathrm{m}], \\ &k = \sigma_C\sqrt{r/2h}\times 10^{-11} \ [\mathrm{F/m}], \\ &f \quad : \text{frequency } [\mathrm{s}^{-1}], \\ &r \text{ and } h \ : \text{conductor radius and height } [m], \\ &\sigma_G = \sigma_C(f+25), \\ &\sigma_C \quad : \text{corona loss constant}. \end{aligned}\right\} \qquad (2)$$

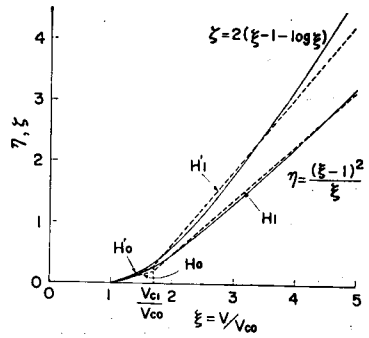

Fig. 1. ξ-η and ξ-ζ curves and those piecewise linear approximations.

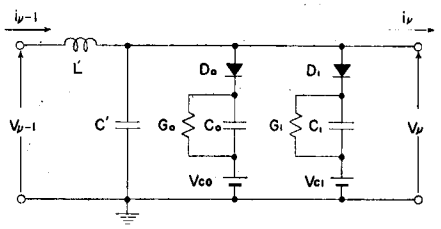

Fig. 2. The ν-th element of an approximate equivalent circuit of a single-conductor system with corona loss elements.

When the two $\xi-\eta$ and $\xi-\zeta$ curves, which are given by Eqs. (2), are linealized piecewise by the two continued rectilinear segments respectively as shown in Fig. 1, the ν-th element of the approximate equivalent circuit of a single-conductor system with the corona loss elements becomes as illustrated in Fig. 2, where $\nu=1, 2, \cdots, n$,

v_ν and i_ν : output voltage and current of the ν-th element,
$v_{\nu-1}$ and $i_{\nu-1}$: input voltage and current of the ν-th element or output ones of the (ν-1)-th,
v_{c1} : voltage at intersection of piecewise rectilinear characteristics,
n : number of total elements.

If we choose the lumped distance of the ν-th element Δx, L' and C' are given by

$$\left.\begin{aligned} L' &= L\Delta x \\ C' &= C\Delta x \end{aligned}\right\} \qquad (3)$$

and, if we assume the slope of the two continued rectilinear segments of $\xi-\eta$ curves are H_0, H_1 and those of $\xi-\zeta$ curves are H_0', H_0' respectively, the equivalent leakances G_0, G_1 and equivalent capacitances C_0, C_1 are given by

$$\left.\begin{aligned} G_0 &= KH_0\Delta x \\ G_1 &= K(H_1-H_0)\Delta x \end{aligned}\right\} \qquad (4)$$

$$\left.\begin{aligned} C_0 &= kH_0'\Delta x \\ C_1 &= k(H_1'-H_0')\Delta x \end{aligned}\right\} \qquad (5)$$

respectively.

But, the value of the line voltage may transiently become both the positive

and negative, though it is assumed to be always positive in our case, then we must add the inverse-polarity and hysteresis elements to the corona loss ones, in Fig. 2.

Next in respect to the equivalent circuit element shown in Fig. 2, we conveniently define modes 0, 1 and 2 as follows;

$$\left.\begin{aligned} &\text{Circuit mode in} \quad 0 \leq v_\nu < v_{c0} \quad = \text{mode } 0\,, \\ &\text{Circuit mode in} \quad v_{c0} \leq v_\nu < v_{c1} = \text{mode } 1\,, \\ &\text{Circuit mode in} \quad v_{c1} \leq v_\nu \quad = \text{mode } 2\,, \end{aligned}\right\} \tag{6}$$

where it is, too, assumed that the value of the transient voltage is positive.

2.2. Approximate Difference Equations and Those New Numerical Analysis

We have the following difference-differential equations concerning x and t for the input and output voltages and currents of the ν-th element in Fig. 2. If the ν-th element is in mode 2.

$$\left.\begin{aligned} &L'\frac{di_{\nu-1}}{dt} = v_{\nu-1}-v_\nu\,, \\ &C'\frac{dv_\nu}{dt}+C_0\frac{d(v_\nu-v_{c0})}{dt}+G_0(v_\nu-v_{c0}) \\ &\qquad +C_1\frac{d(v_\nu-v_{c1})}{dt}+G_1(v_\nu-v_{c1}) = i_{\nu-1}-i_\nu\,, \\ &\nu = 1, 2, \cdots, n\,. \end{aligned}\right\} \tag{7}$$

From Eqs. (7), we can introduce the next approximate difference equations concerning x and t.

$$\left.\begin{aligned} &L''(i_{\nu-1}-i_{\nu-1}^0) = v_{\nu-1}-v_\nu\,, \\ &C''(v_\nu-v_\nu^0)+C_0'(v_\nu-v_\nu^0)+G_0(v_\nu-v_{c0}) \\ &\qquad +C_1'(v_\nu-v_\nu^0)+G_1(v_\nu-v_{c1}) = i_{\nu-1}-i_\nu\,, \end{aligned}\right\} \tag{8}$$

where

$$\left.\begin{aligned} &L'' = L'/\Delta t,\ C'' = C'/\Delta t,\ C_0' = C_0/\Delta t,\ C_1' = C_1/\Delta t\,, \\ &v_\nu^0 = v_\nu|_{t=t-\Delta t}\,, \qquad t \geq 0\,, \\ &i_{\nu-1}^0 = i_{\nu-1}|_{t=t-\Delta t}\,, \quad t \geq 0\,, \\ &\nu = 1, 2, \cdots, n\,. \end{aligned}\right\}$$

Assuming the recurrence relations between voltages and currents to be as follows,

$$\left.\begin{aligned} i_\nu &= a_{2\nu}v_\nu+b_{2\nu}\,, \\ v_\nu &= a_{2\nu-1}i_{\nu-1}+b_{2\nu-1}\,, \end{aligned}\right\} \tag{9}$$

then, from Eqs. (8) and Eqs. (9) we can get the following expressions with respect to the coefficients.

$$\left.\begin{aligned} a_{2\nu} &= 1/(L''+a_{2\nu+1}) \,, \\ b_{2\nu} &= (L'' i_\nu^0 - b_{2\nu+1})/(L''+a_{2\nu+1}) \,, \\ a_{2\nu-1} &= 1/(C''+C_0'+C_1'+G_0+G_1+a_{2\nu}) \,, \\ b_{2\nu-1} &= \{(C''+C_0'+C_1')\, v_\nu^0 + (G_0 v_{c0}+G_1 v_{c1}-b_{2\nu})\} \\ &\qquad /(C''+C_0'+C_1'+G_0+G_1+a_{2\nu}) \,. \end{aligned}\right\} \tag{10}$$

The above mentioned discussions are applicable to the case, where the ν-th element is in mode 2, and moreover we may assume that $C_1'=G_1=0$ in Eqs. (10), if the ν-th element is in mode 1, and that $C_0'=C_1'=G_0=G_1=0$, if in mode 0.

Then we can get the recurrence formula of each coefficient a_m and b_m as given in Eqs. (11).

(i) When m is odd:

$$\left.\begin{aligned} a_{m-1} &= 1/(L''+a_m) \,, \\ b_{m-1} &= (L'' i^0_{(m-1)/2} - b_m)/(L''+a_m) \,. \end{aligned}\right\}$$

(ii) When m is even:

(a) If the $m/2$ element is in mode 0,

$$\left.\begin{aligned} a_{m-1} &= 1/(C''+a_m) \,, \\ b_{m-1} &= (C'' v^0_{m/2} - b_m)/(C''+a_m) \,. \end{aligned}\right\}$$

(b) If the $m/2$ element is in mode 1, (11)

$$\left.\begin{aligned} a_{m-1} &= 1/(C''+C_0'+G_0+a_m) \,, \\ b_{m-1} &= \{(C''+C_0')\, v^0_{m/2} + (G_0 v_{c0} - b_m)\} \\ &\qquad /(C''+C_0'+G_0+a_m) \,. \end{aligned}\right\}$$

(c) If the $m/2$ element is in mode 2,

$$\left.\begin{aligned} a_{m-1} &= 1/(C''+C_0'+C_1'+G_0+G_1+a_m) \,, \\ b_{m-1} &= \{(C''+C_0'+C_1')\, v^0_{m/2} + (G_0 v_{c0}+G_1 v_{c1}-b_m)\} \\ &\qquad /(C''+C_0'+C_1'+G_0+G_1+a_m) \,. \end{aligned}\right\}$$

Furthermore, see the Appendix of Reference [5] for the criteria of the mode transitions.

On the other hand, at the final end ($\nu=n$) the relation between the voltage v_n and current i_n will be generally given by,

$$i_n = a_{2n} v_n + b_{2n} \tag{12}$$

where a_{2n} and b_{2n} are constants to be determined by terminal condition.

Substituting the numerical values of a_{2n}, b_{2n}, the line constants, terminal conditions etc. into recurrence formula Eqs. (11) deduced as above, we can calculate the numerical values of a_{2n-1}, b_{2n-1}, $\cdots$, a_0, b_0 with digital computer. And after obtaining each coefficient a_m, b_m, we can seek the values of the voltages v_ν and currents i_ν for $\nu=1, 2, \cdots, n$ with Eqs. (9). Lastly, a digital computer flow-chart is drawn in Fig. 3.

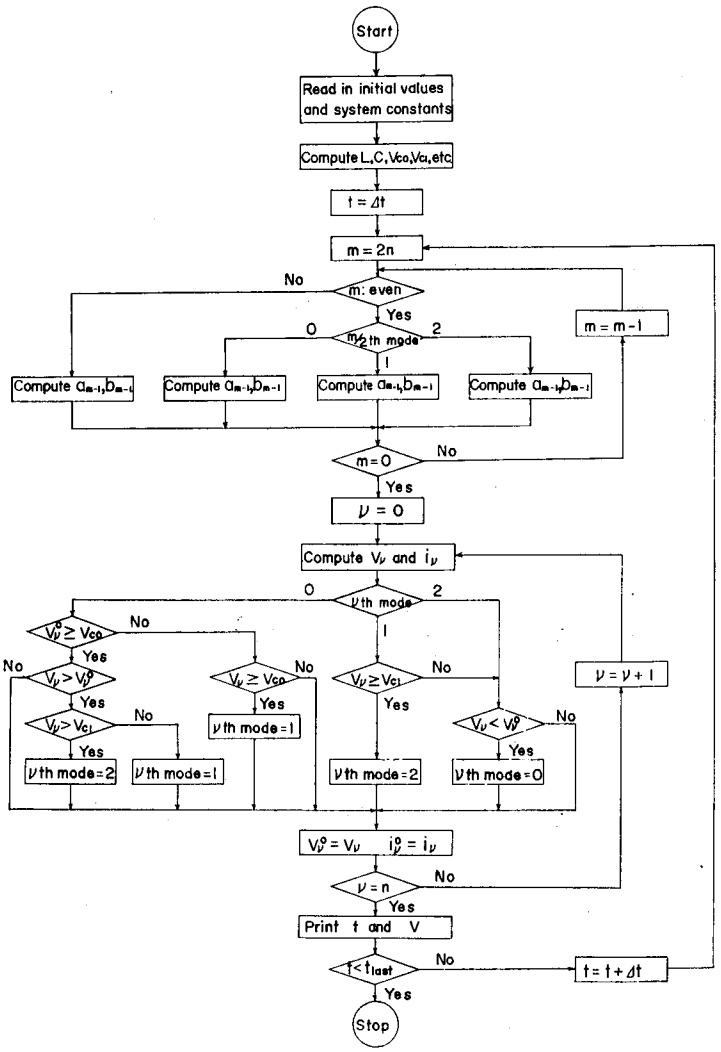

Fig. 3. Digital computer flow-chart.

3. Numerical Calculations and Estimations of Corona Loss Constants

3.1 Numerical Conditions

In this section, the numerical values of the system constants given in the Reference [5] are used in the computations, since we intend to obtain the optimum values of the corona-loss constants σ_C and σ_G by comparing the results, which are obtained by the digital computation method described in the previous article, with the experimental ones given by Aso and Fujitaka.

Table 1. Values of main quantities availed in computations.

Line length: l	2067	[m]
Hight of conductor: h	3.1	[m]
Radius of conductor: r	1.15×10^{-3}	[m]
Lumped distance: Δx	51.7	[m]
Time duration: Δt	0.005	[μs]
Surge impedance of line: z	516	[Ω]
Inductance of conductor: L	1.72	[μH/m]
Capacitance of conductor: C	6.47	[$\mu\mu$F/m]
Number of equivalent circuit elements: n	40	
Corona voltage: v_{c0}	28.3	[kV]
Break point voltage: v_{c1}	48.1	[kV]

Table 1 shows the values of the constants used in the calculations. The value of v_{c0} is computed from the following equation.

$$v_{c0} = m_0 m_1 \delta g_0 r \times 10^{-11}/(18C)\,, \tag{13}$$

where

m_0 : surface coefficient of conductor (=0.96),
m_1 : weather factor (=1),
δ : relative density of air (=1),
g_0 : insulation breakdown strength of air (=2980 KV/m),
r : radius of conductor ($=1.15\times10^{-3}$ m),
C : capacitance per unit length of conductor
($=6.47$ $\mu\mu$F/m).

Moreover, $v_{c1}=1.7\ v_{c0}$ is adopted by considering the input impulse peak

voltage and the shape of ξ-η, ξ-ζ curves. And the computation is carried out on the assumption that K and k and hence σ_G and σ_C are independent of each other. Since the equivalent frequency f with respect to the travelling wave is uncertain, this treatment may be considered as proper.

3.2 Estimations of Optimum Values of σ_C and σ_G

The computations were carried out according to the above principles. In Fig. 4 are plotted the digital calculation results of the transient voltages at the final end, which are grounded with the surge impedance of the line, about the various values of σ_C and σ_G. Also, Fig. 4 (a–1)$\sim$(a–3) show the final end voltage waveforms in repsect to the positive applied impulses, whose wave tail time constants are 5 μs, 20 μs and 80 μs respectively, and Fig. 4 (b–1)$\sim$(b–3) show those corresponding to the negative ones.

From these figures, we can see that the waveforms similar to the actual corona distortion of the surges can be obtained. However, as previously described, because of the use of piecewise linear approximation for the ξ-η and ξ-ζ curves in our computation, it is unavoidable that the step shapes appear at the vicinity of the braek-point voltage v_{c1} in the voltage waveforms. Furthermore, from Fig. 4 it may be said that the time lag of wavefront increases if the value of σ_C does, on the other hand, the attenuation of the crest increases if the value of σ_G does. Finally, we could obtain the values of σ_C and σ_G shown in Table 2, as the optimum values of them, by comparing the computed results shown in Fig. 4 and another computed ones, though we don't illustrate the latter in this paper, with the experimental results by Aso and Fujitaka.

Next, some examples calculated with the estimated values of σ_C and σ_G given in Table 2, are shown by the solid lines in Fig. 5. For comparison, the corresponding experimental waveforms by Aso and Fujitaka are also shown by the dotted line in the same figure. It will be seen that the computed results the attenuation of the peak value and the distortion of the waveform are in good agreement with the experimental ones. However, in the figure, the computed and

Table 2. Optimum values of σ_C and σ_G for positive and negative surges.

Wave tail time constant	Positive surge		Negative surge	
	σ_C	σ_G	σ_C	σ_G
$\tau=5\ \mu$s	32	30×10^6	17	18×10^6
$\tau=20\ \mu$s	32	18×10^6	17	18×10^6
$\tau=80\ \mu$s	25	27×10^6	12	27×10^6

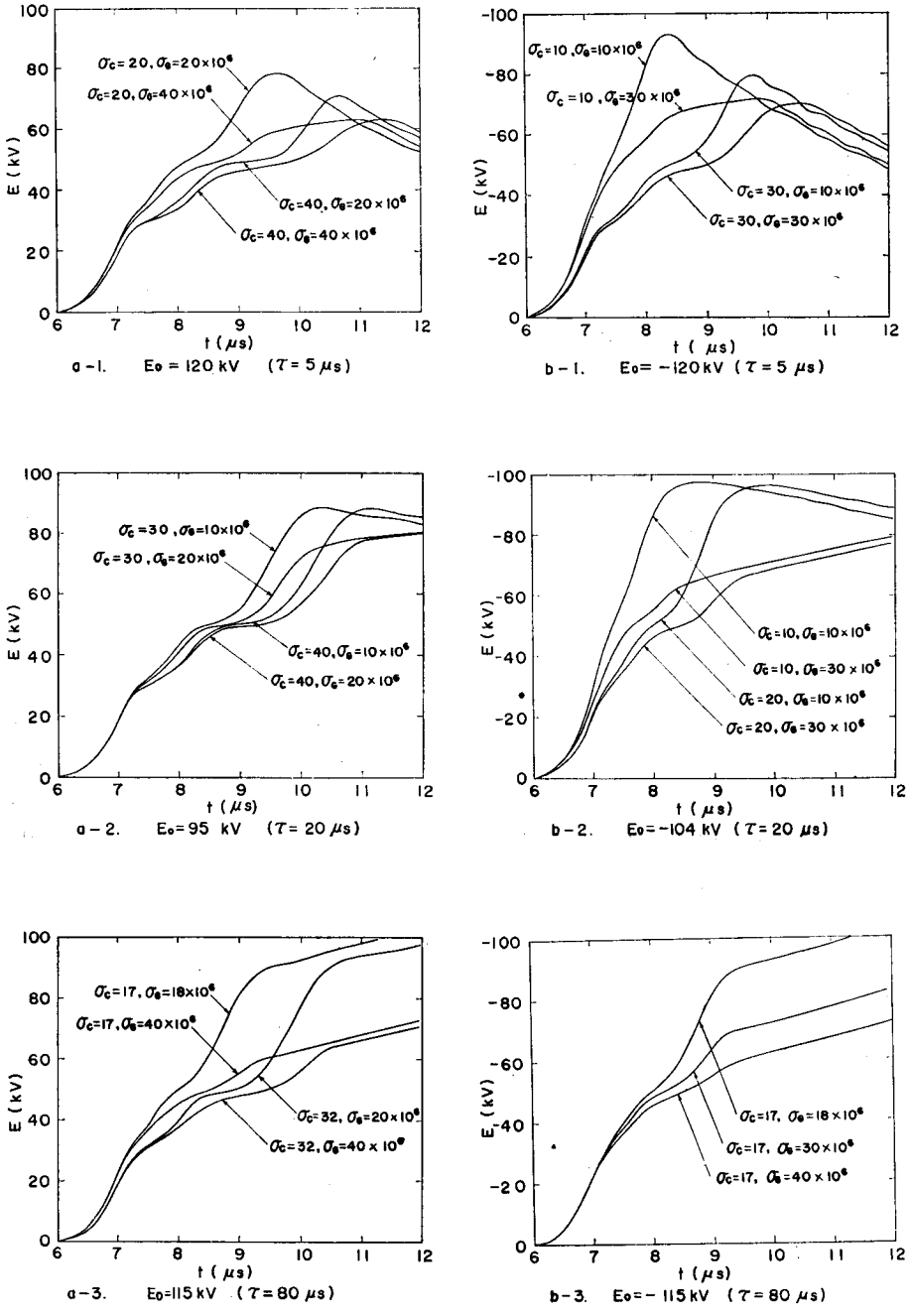

Fig. 4. Digital computation results of final end voltage waveforms corresponding to the various values of σ_Q and σ_G.

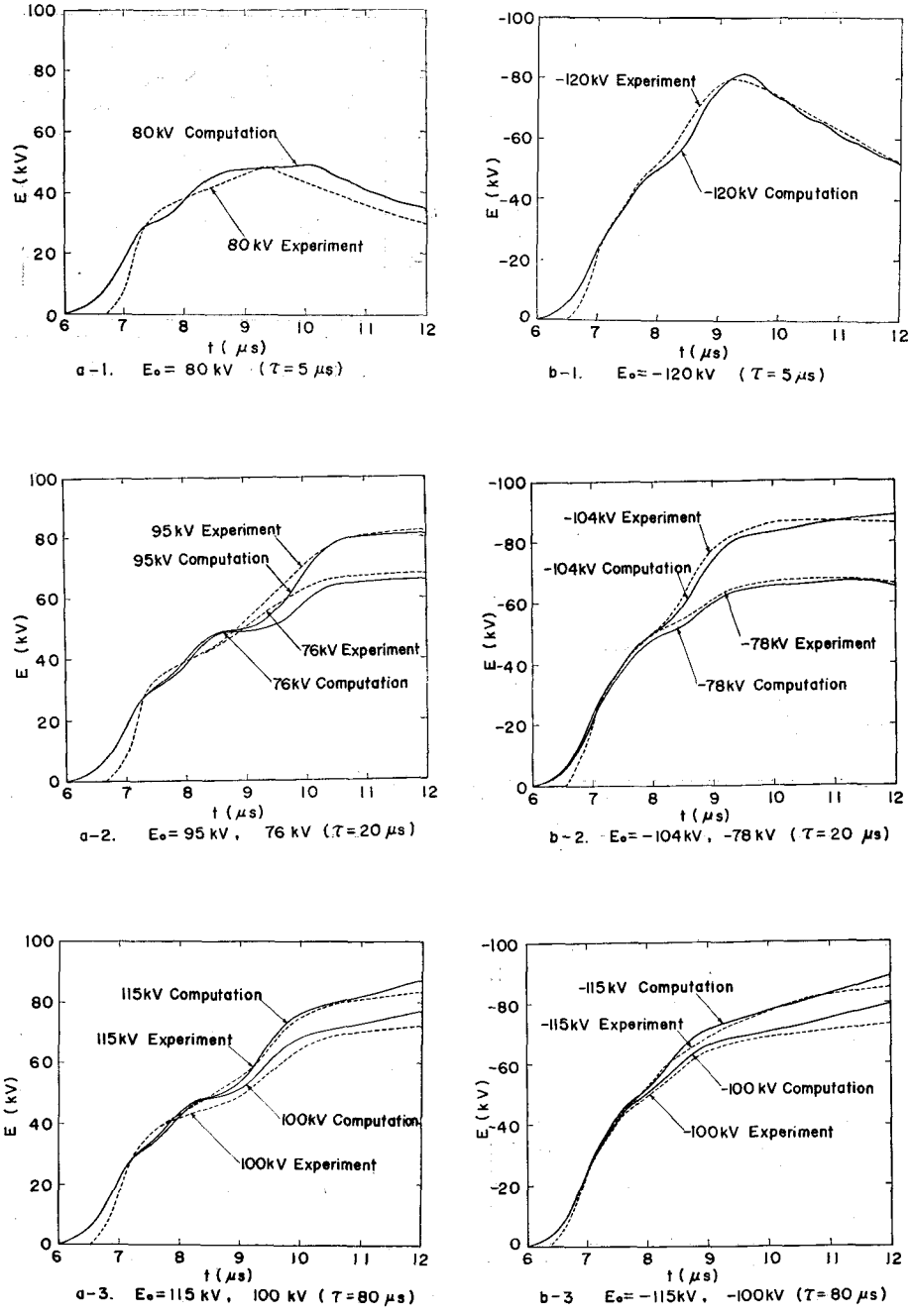

Fig. 5. Comparison of computed and experimental examples of final end voltages.

experimental waveforms are plotted such that both coincide at the instant when the corona voltage (calculated value) is reached because the experimental wavetoes slope somewhat larger than the computed ones. Moreover, the calculated waveforms have had larger distortion than the experimental results immediately after the arrival of the corona voltage, due to the fact that the slope of the first line segment is larger than the slope of the actual ξ-ζ curve. As previously described, since the piecewise rectilinear approximation is used, the step phenomena at the vicinity of the break-point voltage are unavoidable.

3.3 Comparison with the Computed Results by Surge Analyser

The authors have already estimated the other optimum values of σ_C and σ_G for the surge (wave tail time constant $\tau=20$ μs) by surge analyser. They were

$$\sigma_C \simeq 40\,, \quad \sigma_G \simeq 4.5\times 10^6 \quad : \text{positive surge,}$$
$$\sigma_C \simeq 20\,, \quad \sigma_G \simeq 5.5\times 10^6 \quad : \text{negative surge.}$$

Comparing the estimated values by digital computer with those by surge analyser, we can see that the value of σ_G considerably differs. Fig. 6 shows one computed result of the final end voltage by surge analyser, and that by digital computer under the same conditions. From the figure it can be seen that the peak value of voltage waveform computed by surge analyser is more attenuated than that of digital computer. It is due to the fact that the resistance losses of the inductance coils are unavoidable in the surge analyser. Therefore, it seems to be natural that the difference arises between the two estimated values of σ_G.

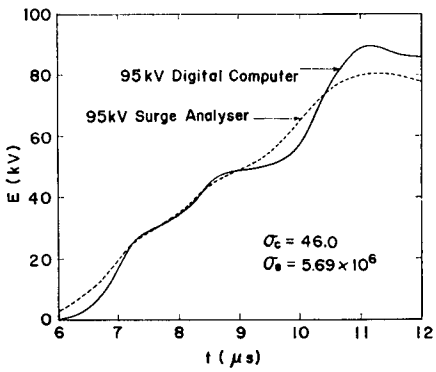

Fig. 6. Comparison of computed results by digital computer and by surge analyser.

4. Conclusion

In the preceding sections have been presented a new numerical analysis of the attenuation and distortion of the surges due to corona discharges on a single-conductor system. Furthermore, the practical various computations were carried out by digital computer, and the computed results were compared with the experimental results, which have been obtained by Aso and Fujitaka. From the comparisons, the optimum values of σ_C and σ_G were selected for the positive and

negative surge. And it may be considered that they are more accurate than the ones previously estimated by surge analyser. And all these computations were done by KDC-II in the Kyoto University Computation Center.

Finally, since actual transmission systems are multi-conductor systems, we are now performing the digital computations expanded to the multi-conductor. All of these we will reserve for another occasion.

Acknowledgment

The authors wish to express their appreciation to professor S. Hayashi of Dōshisha University and Mr. E. Nakamura of Sumitomo Electric Industries, Ltd.

References

1) S. Hayashi, J. Umoto and S. Machida; Convention records at the annual meeting of I.E.E.J., No. 565, May (1958).
2) S. Hayashi and J. Umoto; Convention records at the annual meeting in Kansai District of I.E.E.J., No. 98, Oct. (1958).
3) S. Hayashi, J. Umoto and E. Nakamura; Ibid, No. 9–9, Nov. (1964).
4) S. Hayashi, J. Umoto and E. Nakamura; J.I.E.E.J., **86**, 108 114, Jan. (1966).
5) S. Hayashi, J. Umoto and E. Nakamura; Memoirs of the Faculty of Engineering, Kyoto University, Vol. XXV, part 2 Apr. (1966).
6) T. Aso and S. Fujitaka; J.I.E.E.J. **74**, 1211 1217, Oct. (1954)